Materials Today Bio 31 (2025) 101473

Contents lists available at ScienceDirect

Materials Today Bio

journal homepage: www.journals.elsevier.com/materials-today-bio

Bivalirudin functionalized hydrogel coating capable of catalytical NO-generation for enhanced anticorrosion and biocompatibility of magnesium alloy

Changjiang Pan [a,1,*], Naiquan Yang [b,1], Jie Chen [c], Qiuyang Zhang [c], Linhong Deng [a], Teng Luo [a], Lingjie Meng [c]

[a] School of Medical and Health Engineering, Institute of Biomedical Engineering and Health Sciences, Changzhou University, Changzhou, 213164, China
[b] Department of Cardiology, The Affiliated Huai'an Hospital of Xuzhou Medical University, Huai'an, 223003, China
[c] Faculty of Mechanical and Material Engineering, Jiangsu Provincial Engineering Research Center for Biomaterials and Advanced Medical Devices, Huaiyin Institute of Technology, Huai'an, 223003, China

ARTICLE INFO

Keywords:
Magnesium alloy
Hydrogel
Blood compatibility
Endothelialization

ABSTRACT

Magnesium and its alloys are undoubtedly ideal candidates for manufacturing new bioabsorbable vascular stents thanks to their good bio-absorbability and better mechanical characteristics. However, the bottlenecks that restrict their clinical application, such as fast corrosion *in vivo*, poor hemocompatibility, and inferior surface endothelial regeneration ability, have not been resolved fundamentally. In this study, a polydopamine (PDA) intermediate layer covalently linked with acrylamide was first constructed on the alkali-heat-treated magnesium alloys, followed by *in-situ* polymerizing methacryloyloxyethyl sulfonyl betaine (SBMA) and acrylamide (AAM) to fabricate a hydrogel coating on the surface by ultraviolet (UV) polymerization. Finally, bivalirudin and selenocystamine were sequentially grafted onto the hydrogel coating surface to construct a multifunctional bioactive corrosion-resistant coating with excellent antifouling, anticoagulant performance, and catalytic liberation of NO (nitric oxide) to facilitate endothelial cell (EC) growth. The outcomes verified that the bioactive coating could not only significantly resist corrosion of magnesium alloys, but also had excellent hydrophilicity and the ability to selectively promote albumin adsorption, which could prevent platelet adhesion and activation and significantly diminish the hemolysis occurrence, thereby considerably facilitating its anticoagulant properties. At the same time, due to the hydrophilicity and extracellular matrix-like characteristics of the hydrogel coating, the coating could promote EC growth and upregulate the secretion of vascular endothelial growth factor (VEGF) and NO of endothelial cells (ECs). In the case of catalytic NO-liberation, the catalytic release of NO could further significantly improve blood compatibility, EC growth, and functional expressions of ECs. Therefore, the method in this study provides an effective strategy to fabricate the bioactive hydrogel coating that can simultaneously resist corrosion and enhance the biocompatibility of magnesium-based alloys, thereby effectively promoting research and application of magnesium alloy in intravascular stents.

1. Introduction

Medical magnesium and its alloys are undoubtedly ideal candidates for developing new biodegradable vascular stents owing to their good bio-absorbability and excellent mechanical characteristics [1]. However, the fast corrosion *in vivo* and the inferior biocompatibility that restrict their clinical application have not been addressed thoroughly [2]. In particular, as a biodegradable metal used in intravascular implants, the rapid degradation caused by the complicated physiological environment *in vivo* usually leads to poor surface anticoagulant performances and inferior endothelial regeneration ability [3,4], which still have no fundamental solution at present, resulting in a lot of clinical issues, such as in-stent restenosis (ISR) and late thrombus. Studies have verified that the excessive corrosion products (Mg^{2+}, H_2, $Mg(OH)_2$, etc.)

This article is part of a special issue entitled: Surface & Interface published in Materials Today Bio.

* Corresponding author.
E-mail address: pcj@cczu.edu.cn (C. Pan).

[1] These authors contributed equally to this work.

https://doi.org/10.1016/j.mtbio.2025.101473
Received 14 October 2024; Received in revised form 14 November 2024; Accepted 8 January 2025
Available online 11 January 2025

produced by the rapid degradation and the limited surface bioactivity play a significant role in the anticoagulant properties and reendothelialization of the magnesium-based alloy surface [5,6]. Although great advances in the enhancement of anticorrosion have been achieved through chemical treatment [7], electrochemical treatment [8], preparation of inorganic non-metallic and polymer coatings [9], and composite coatings [10,11], the poor anticoagulant properties and weak reendothelialization ability aroused by the fast corrosion have been improved to some degree. Additional surface bio-functionalization or loading of bioactive factors on these surface-modified layers can further improve their biocompatibility and *in vivo* service effect [12,13]. However, at present, the binding force between most surface-modified layers and the magnesium substrate is relatively weak, and the preparation process of the coating is also relatively complex and time-consuming [9,14]. Furthermore, with the gradual biodegradation of the surface coating and the premature loss of biomolecules, it is difficult to adapt to the physiological and pathological processes within the blood vessels, which may still lead to the occurrence of blood coagulation or delayed reendothelialization. Therefore, with the aim of achieving a perfect adaption between degradation and biocompatibility, discovering new surface modification ways to augment the anti-corrosion properties and biocompatibility of magnesium-based alloys is urgently needed.

Hydrogel, with a structure similar to the extracellular matrix (ECM), is a network polymer that can hold lots of water without dissolving. It has good biocompatibility, especially its three-dimensional (3D) porous network structure is very suitable for cell metabolism and tissue growth. Therefore, hydrogel has been widely explored in biomaterials, injectable hydrogel drugs, drug delivery systems, and tissue engineering [15,16]. The preparation strategies of hydrogel mainly utilize physical (hydrogen bond, electrostatic interaction, hydrophobic force, etc.) or chemical (covalent crosslinking) interactions between natural polymers or synthetic polymers to form a 3D crosslinked network structure [17]. The hydrogel prepared by physical crosslinking often has an inferior intermolecular binding force, which is generally reversible and has good biocompatibility and degradability. However, its mechanical strength is limited and its stability in complicated physiological environments is not good enough. The hydrogel formed by chemical crosslinking usually has covalent bonds between the polymer segments, resulting in better mechanical strength and stability; however, the biocompatibility may be lessened, often requiring further biofunctionalization. Although hydrogels have been extensively explored in biomedical materials and scaffolds for tissue engineering, the direct application of current hydrogels for surface modification of magnesium alloys has the disadvantages of weak binding force with substrate and difficulty in further biological modification. In our previous work [18], a polydopamine (PDA) layer was first prepared on the alkali-heat-treated magnesium alloy surface, then sodium alginate/carboxymethyl chitosan (SA/CMCS) hydrogel was immobilized on the surface, followed by the respective grafting of selenocystamine and CO-releasing molecule (CORM401) to obtain hydrogel coatings that could catalyze the liberation of NO or CO, the results demonstrated that the corrosion-resisting properties and biocompatibility were augmented obviously.

Ultraviolet (UV)-polymerization represents an effective and facile way for *in-situ* fabrication of hydrogel coatings on the biomaterial surface [19]. Compared with other methods, UV-polymerization has the advantages of fast reaction speed, low operating costs, and simple equipment. Chen et al. [20] fabricated a poly (2-methacryloyloxyethyl phosphocholine) (PMPC) coating on the magnesium alloy surface by the thiol-ene UV polymerization, significantly enhancing the anticorrosion properties in simulated body fluid (SBF) and effectively inhibiting platelet adhesion. However, strictly speaking, this coating cannot be called a hydrogel coating because only one molecule of MPC was polymerized on the surface and the coating has no cross-linking structure. Moreover, PMPC is not conducive to cell growth, thus its application for stents is limited. In the present study, a PDA coating containing acrylamide (AAM) was first fabricated on the magnesium alloy (AZ31B) surface, and methacryloyloxyethyl sulfonyl betaine (SBMA) and acrylamide were copolymerized on the Mg surface using UV polymerization to construct a hydrogel coating (SBMA/2AAM) that had excellent antifouling property and could promote endothelial growth. The hydrogel coating was covalently linked to the surface C=C groups. Combining the property of the strong binding force of the polydopamine with the substrate, the hydrogel coating prepared in this study has a good binding force with the substrate and is stable in the physiological environment. To further improve the anti-corrosion and biocompatibility, bivalirudin (a direct thrombin inhibitor) and selenocystamine capable of catalytical NO liberation from the NO donor were sequentially immobilized on the hydrogel coating surface, thereby constructing an anticoagulant hydrogel coating that can catalyze the NO generation (Fig. 1A and B). Due to the excellent hydrophilicity of the as-prepared hydrogel coating, the hemocompatibility of bivalirudin, and the promotion of endothelial regeneration of NO, the bioactive coating constructed in this study could significantly augment the anticorrosion, anticoagulant properties, and EC growth of the Mg alloy (Fig. 1C).

2. Materials and methods

2.1. Materials and reagents

The AZ31B magnesium alloy was provided by the Institute of Metal Research of the Chinese Academy of Sciences. Methacryloyloxyethyl sulfonyl betaine (SBMA), acrylamide, dopamine were purchased from Shanghai Aladdin Biochemical Technology Co., Ltd. Bivalirudin, 1-ethyl-(3-dimethyl aminopropyl) carbodiimide hydrochloride (EDC), N-hydroxysuccinimide (NHS), glutathione (GSH), S-nitrosoglutathione (GSNO), rhodamine, and 4,6-diamidino-2-phenylindole (DAPI) were bought from Sigma-Aldrich (Shanghai, China). CORM-401 was obtained from MedChemExpress (Shanghai, China). The GMP-140 was provided by Easy Biotech (Shanghai) Co., Ltd. The NO and VEGF kits were bought from Beyotime Biotech Inc. (Shanghai, China) and Quanzhou Juang Biotechnology Co., Ltd, China, respectively. The cell culture medium was purchased from Thermo Fisher Scientific Inc.

2.2. Fabrication of a bioactive hydrogel coating capable of catalytical NO release

The chemical structures of SBMA, acrylamide, bivalirudin, and selenocystamine are shown in Fig. 1A. Fig. 1B illustrates the preparation process of the bioactive hydrogel coating on the surface. AZ31B magnesium alloy platelets (Mg, 12 mm diameter, 5 mm thickness) were ground and washed, then treated for 24 h at 75 °C by immersing them in a 3 M NaOH solution, and the samples were named Mg-OH. To obtain a PDA intermediate layer containing C=C groups, Mg-OH was placed in a mixed solution of dopamine (2 mg/mL) and acrylamide (2 mg/mL) (pH 8.5, the volume ratio was 2:1.) to oscillate for 8 h, it was designated as Mg-DAM. For UV polymerization, a mixture of SBMA (100 μL, 5 wt %) and acrylamide (100 μL, 10 wt %) was evenly covered on Mg-DAM surface and then irradiated with UV light (357.8 W) for 8 min. After washing with deionized water, the hydrogel coating (Mg-SBMA/2AAM) was obtained.

To obtain the anticoagulant hydrogel coating with the ability of catalytical NO-generation, bivalirudin and selenocystamine were sequentially introduced onto the hydrogel coating. Bivalirudin is an anticoagulant peptide containing many carboxyl and amine groups. The carboxyl group can be activated by carbodiimide with the help of N-hydroxysuccinimide (NHS) to form a succinimide group, which can easily form an amide bond with the amine groups of acrylamide and selenocystamine, so that bivalirudin and selenocystamine can be successively immobilized on the magnesium alloy surface modified by SBMA/2AAM hydrogel coating. For the grafting of bivalirudin, the Mg-SBMA/2AAM was immersed in 20 mL bivalirudin solution (3 mg/mL), then 0.14 g EDC and 0.05 g NHS were placed into the solution for

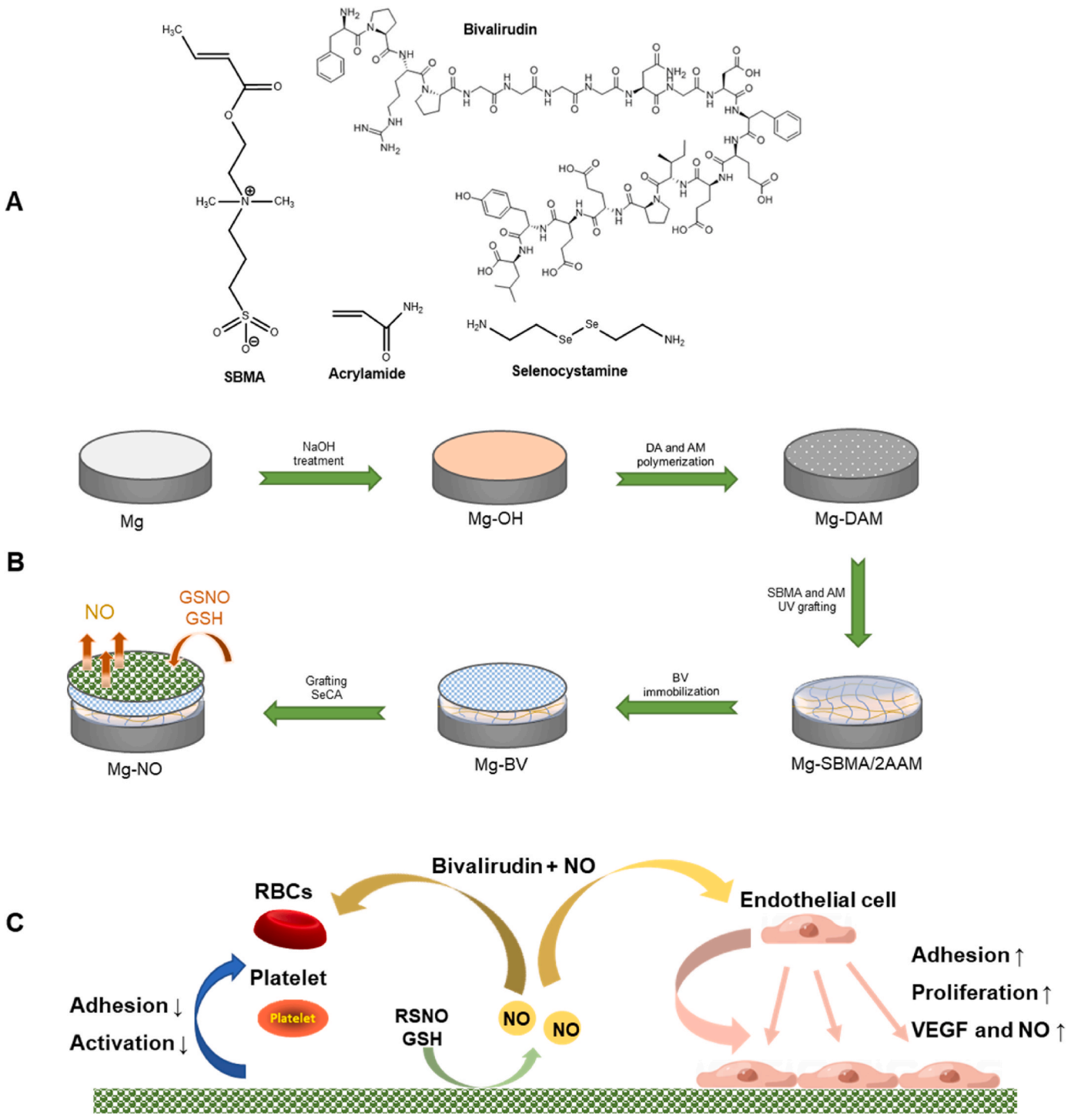

Fig. 1. The chemical structures of SBMA, acrylamide, bivalirudin, and selenocystamine (A), and the scheme of the construction route of the biomimetic coating that can catalyze the NO-generation (B) and its mechanism for improving biocompatibility (C).

reacting for 4 h at room temperature, the obtained sample was named Mg-BV. The selenocystamine was immobilized on the Mg-BV surface using the same method. Briefly, the Mg-BV was placed into 20 mL selenocystamine dihydrochloride (3 mg/mL, in Tris HCl buffer, pH 8.5), then 0.14 g EDC and 0.05 g NHS were added to activate the carboxyl groups of Mg-BV to form succinimide groups, which can be covalently linked with amine groups of selenocystamine. After reaction for 10 min at room temperature, the sample was cleaned and labeled as Mg-NO.

2.3. Surface characterization

The changes in chemical structures of the varying specimens were examined and analyzed by ATR-FTIR (Perkin Elmer Paragon 2000) and XPS (Thermo Fisher Scientific K-Alpha, United States). The surface morphologies after surface modification and the surface corrosion morphologies at different corrosion intervals were observed and analyzed by field emission scanning electron microscopy (FESEM, FEI Quata 250, United States). The hydrophilicity was investigated by measuring the water contact angle (WCA).

2.4. Electrochemical corrosion and degradation behaviors

The electrochemical corrosion behaviors of varying modified materials were characterized by measuring the potentiodynamic polarization (PDP) curve and electrochemical impedance spectroscopy (EIS) utilizing the three-electrode system on an electrochemical workstation (CHi660D, CHI Instruments, Inc, China), which consisted of working (sample), auxiliary (platinum wire), and reference (saturated calomel) electrodes. The measurement was carried out in 250 mL SBF in an electrolytic cell with a scanning speed of 1 mV/s. The Tafel extrapolation method was applied to acquire the corrosion parameters (corrosion potential (E_{corr}) and corrosion current density (I_{corr})) according to the PDP curve. The corrosion rate was calculated using the equation in the literature [21]. The EIS measurement was carried out by scanning from 10^5 Hz to 0.01 Hz utilizing a sinusoidal alternating current (10 mV amplitude) and the corresponding fitting parameters were acquired using ZView software.

To further characterize the corrosion degradation behaviors of magnesium alloys, the sealed sample (1 cm^2 exposed area) was placed into 20 mL SBF solution (pH 7.4) for different periods. Afterward, the sample was washed and dried, and then the surface morphologies were examined by SEM. In the meantime, during the immersion tests, the pH value of each solution was measured at predetermined intervals using a pH meter. Three parallel specimens were detected and the values were averaged.

2.5. Plasma protein adsorption

The BCA method was implemented to evaluate the protein adsorption behaviors of different surfaces, and two important plasma proteins, i.e., bovine serum albumin (BSA) and fibrinogen (Fib), were applied. The specimens after sterilization were laid in a 24-well plate, and 1 mg/mL BSA and Fib solutions were added to fully adsorb for 2.5 h at 37 °C, respectively. After rinsing with phosphate buffer solution (PBS), the specimens were transferred into another 24-well plate, and 1 mL solution of 1 wt% sodium dodecyl sulfate (SDS) was added for ultrasonic desorption for 0.5 h. Afterward, 200 μL eluent was transferred into a disinfected 96-well plate, and then 100 μL BCA working solution was added to incubate for 20 min at 60 °C. The absorbance was measured at 562 nm to calculate the amount of adsorbed protein from the standard curve.

2.6. Catalytic NO-generation behavior

The Mg-NO sample was placed in a 3 mL PBS solution containing S-nitrosoglutathione (GSNO, NO donor, 10 μM), and glutathione (GSH, reducing agent, 10 μM) was injected to catalyze the NO generation. The specimen was designated as Mg-NO-C. The NO-generation behavior was determined utilizing the nitrate reductase method. At the predetermined time, 50 μL PBS after incubation was mixed with 50 μL Grignard reagent I and 50 μL Grignard reagent II in a 96-well plate. The absorbance values at 540 nm were determined to compute the NO amount according to the standard curve.

2.7. Biocompatibility

For blood and EC tests, GSH (10 μM, 200 μL) and GSNO (10 μM, 200 μL) were injected into the Mg-NO specimen to catalyze NO-generation, and the specimen was denoted as Mg-NO-C.

2.7.1. Blood compatibility

The anticoagulant properties of different specimens were evaluated using platelet adhesion, platelet activation (plasma α-granule membrane protein 140, GMP140), and hemolysis rate. For the detailed procedures, please refer to our previous work [22].

2.7.2. EC growth, VEGF, and NO expressions

Cell adhesion: The disinfected sample was cultivated with 0.5 mL EC suspension (5×10^4 cells/mL, human umbilical vein endothelial cells, ECV304) and 1.5 mL cell culture medium at 37 °C and 5 % CO_2 in an aseptic cell culture plate. After being cultured for 6 h and 24 h, the specimen was washed with physiological saline to remove the non-attached cells. The adhered cells were fixed by 2.5 % glutaraldehyde at 4 °C for 3 h. After washing again, the cells were successively stained with 100 μL rhodamine (10 μg/mL) for 20 min and 100 μL 4,6-diamidino-2-phenylindole (DAPI, 500 ng/mL) for 10 min. At last, the images of the cells were collected utilizing inverted fluorescent microscopy (Carl Zeiss A2) away from light.

EC proliferation: The CCK-8 method was utilized to characterize cell proliferation. ECs were seeded on the surface according to the above methods. After that they were cultured for 6 h and 24 h, respectively, the samples were placed into a new culture plate, and 0.5 mL CCK-8 solution (in 10 % cell culture medium supplemented with 10 % fetal serum albumin) was injected. The cells were cultured for 3.5 h at 37 °C. In the end, 200 μL culture medium was moved into a new 96-well plate and the absorbance value was determined at 450 nm.

VEGF expression: The VEGF expression of ECs during cell growth was evaluated using the enzyme-linked immunosorbent assay (ELISA) method. ECs were cultured with different surfaces for 6 h and 24 h, respectively. The VEGF was detected using a commercial VEGF ELISA kit. The test was strictly conducted according to the kit instructions.

NO expression: ECs were inoculated onto the sample surface and cultured as described above. The nitric acid reductase method was utilized to measure the NO amount secreted by ECs. The measurement method was the same as the above NO-generation experiment.

2.8. Statistical analysis

At least three parallel samples were measured in this study for protein adsorption, WCA, hemolysis, platelet activation, and EC growth. The data were expressed as the mean value ± standard derivation (SD). The outcomes were analyzed using the one-way variance analysis, and $^*p < 0.05$, $^{**}p < 0.01$, and $^{***}p < 0.001$ were considered statistically significant.

3. Results and discussion

3.1. Surface characterization

The infrared spectra of the different surface-modified samples are shown in Fig. 2A. It is evident that owing to the lack of organic groups on the unmodified surface, no obvious infrared absorption was detected on its surface. As everyone knows, surface alkali heat treatment of metal generally forms dense oxide or hydroxide coatings on the surface, which could introduce -OH groups [23]. Consequently, a significant infrared absorption of -OH was detected at 3700 cm^{-1} on the Mg-OH sample surface. This peak is of great significance for subsequent surface modification, it can offer the binding sites for self-assembly or dopamine self-polymerization, thereby enhancing the corrosion-resisting properties and the binding strength of the modified layer with the substrate. Dopamine is a small molecule that can self-polymerize on surfaces and is extensively investigated in the surface pretreatment of biomaterials [24]. The structure of the polydopamine (PDA) layer formed under different conditions is slightly different, however, all PDA layers can react with amine or thiol group through the Michael addition or Schiff base reactions [25], which is beneficial for further surface biofunctionalization. The present study utilized this property to produce a PDA intermediate layer containing double bonds (C=C) on the surface by mixing dopamine and acrylamide, the acrylamide was covalently linked with the PDA layer during the self-polymerization, which provided the covalent binding sites for subsequent UV polymerization and thus enhanced the binding strength of hydrogel coating with the

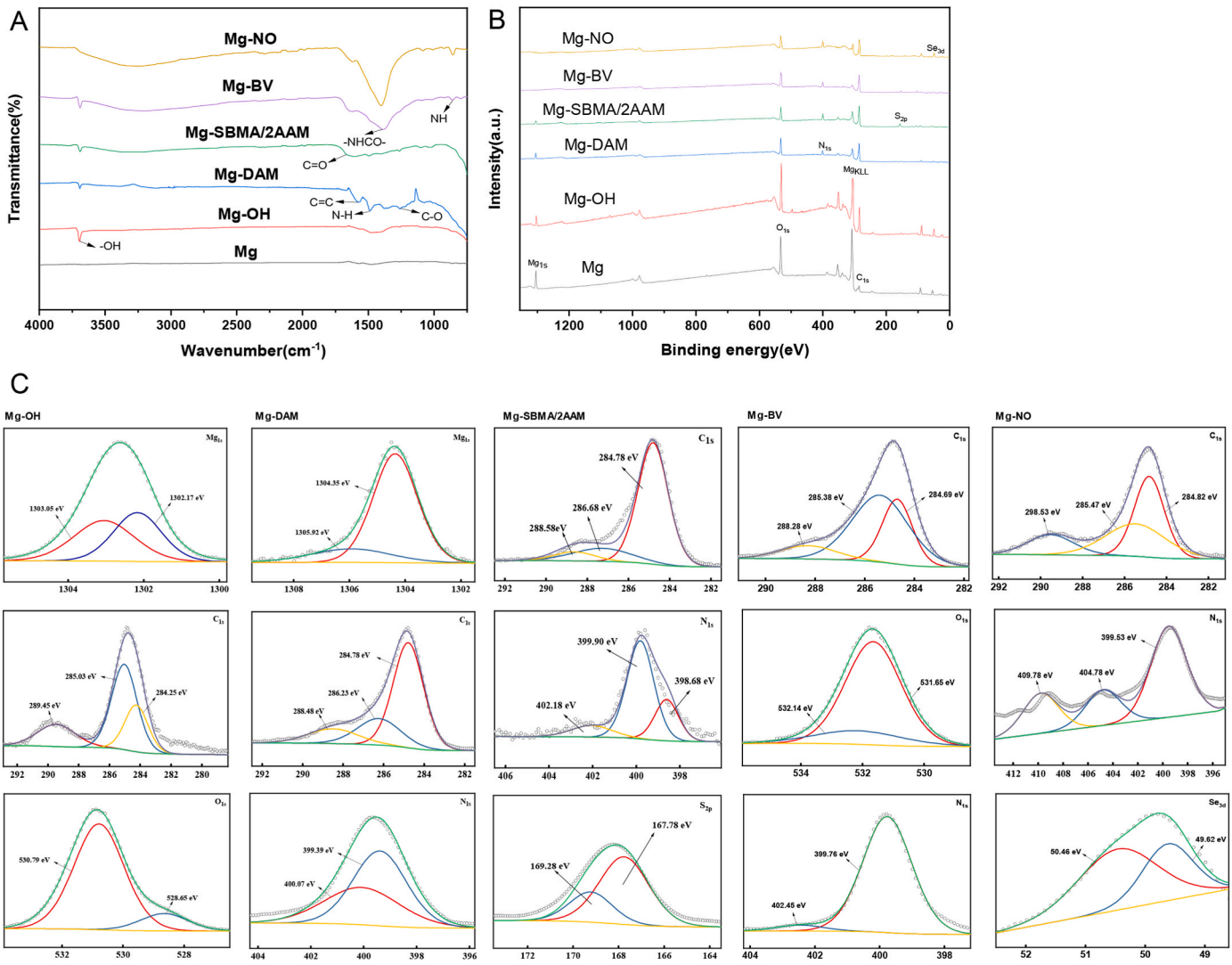

Fig. 2. The infrared spectra (A), XPS survey spectra (B), and XPS high-resolution of some elements of the varying magnesium alloy surfaces.

substrate. As shown in Fig. 2A, after the fabrication of the acrylamide-linked PDA layer (DAM), the absorption peaks at 1280 cm^{-1}, 1489 cm^{-1}, and 1579 cm^{-1} of Mg-DAM could be attributed to the C-O, N-H, and C=C peaks, respectively, demonstrating that the acrylamide had been introduced successfully on the magnesium alloy surface. The introduction of C=C bonds is beneficial for forming covalent bonds with SBMA and acrylamide during the subsequent UV polymerization process, thereby improving the binding force of the hydrogel layer with the substrate. After the fabrication of the SBMA/2AAM hydrogel coating through UV photopolymerization, a C=O group appeared at 1725 cm^{-1} on the surface, while the C=C double bond peak almost completely disappeared, proving that the hydrogel coating was successfully obtained. After covalently grafting the bivalirudin, the surface showed a -NHCO- peak at 1387 cm^{-1} and an NH peak at 861 cm^{-1}, which are the peaks of bivalirudin [26]. In addition, the peak intensity of the O-H/-COOH group at 3700 cm^{-1} was strengthened, suggesting the successful grafting of bivalirudin. After further grafting of selenocystamine, the peak intensity of -NHCO- increased, proving the successful introduction of selenocystamine.

Fig. 2B and C shows the XPS survey spectra and high-resolution images of some elements of the varying surfaces. Table 1 displays the elemental compositions. The Mg surface mainly detected the Mg_{1s} (1303.68 eV), O_{1s} (529.43 eV), C_{1s} (284.82 eV), and a strong Auger peak of Mg (305.08 eV), indicating that the unmodified Mg alloy was very susceptible to oxidation, forming many oxides and some carbon contamination. After NaOH treatment, the characteristic peak of Mg_{1s} weakened and the C and O contents increased, verifying the production of a $Mg(OH)_2$ passivation coating and a few magnesium carbonates on its surface. The spectra of Mg_{1s} and O_{1s} also suggested that the Mg_{1s} had two binding states, corresponding to the hydroxide and carbonate, respectively. A distinct N_{1s} peak appeared on the Mg-DAM sample, the surface carbon content increased significantly and the Mg_{1s} decreased, suggesting that the DAM coating could uniformly cover the surface, which helped improve the corrosion-resisting properties. From the high-resolution spectra of Mg-DAM, C_{1s} could be fitted to C-O (286.23 eV), C-C (284.78 eV), C=C or C=O (288.48 eV) peaks, indicating that

Table 1
The surface element compositions of the varying samples.

Samples	Atomic concentration (at.%)					
	Mg_{1s}	C_{1s}	O_{1s}	N_{1s}	S_{2p}	Se_{3d}
Mg	34.59	7.55	57.86	–	–	–
Mg-OH	14.79	20.74	64.47	–	–	–
Mg-DAM	9.19	43.15	41.22	6.44	–	–
Mg-SBMA/2AAM	2.12	56.87	28.64	8.23	4.14	–
Mg-BV	0.84	57.27	32.10	7.68	2.11	–
Mg-NO	0.54	52.07	37.46	7.79	–	2.68

acrylamide was successfully introduced into the coating during the self-polymerization, which was helpful for subsequent UV covalent polymerization of the hydrogel coating and thus improved the binding strength of the coating with the Mg substrate. The XPS survey spectrum of Mg-SBMA/2AAM exhibited a characteristic S_{2p} (168.25 eV) peak with a content of 4.14 %, which could be attributed to the sulfonic acid groups in SBMA. Meanwhile, the C and N on the surface increased significantly because many carbon and nitrogen were introduced after the polymerization of acrylamide and SBMA. The S element is the characteristic element of SBMA, proving that the SBMA/2AAM hydrogel coating had been successfully constructed on the surface. On the other hand, for Mg-SBMA/2AAM, C_{1s} can be fitted into C-C (284.78 eV), C-O (286.68 eV) and C=O (288.58 eV) peaks, S_{2p} can be decomposed into S-O (167.78 eV) and S=O (169.28 eV), implying that the sulfonic acid group had been successfully introduced on the surface. After bivalirudin was immobilized on the Mg-SBMA/2AAM, the N_{1s} peak slightly decreased, however, the changes in C and O were not obvious. At the same time, due to the grafting of bivalirudin, the proportion of C and O increased, resulting in a decrease of the S element on the surface. The C_{1s} peak can be decomposed into three peaks: the binding energies at 288.28 eV, 285.38 eV, and 284.69 eV, which corresponded to NHCO/COOH, C-N, and C-C, respectively. The N_{1s} spectrum could be fitted into N-C=O (402.45 eV) and C-NH_2 (399.77 eV) [27]. These outcomes suggested that bivalirudin had been immobilized on the hydrogel coating surface. After the grafting of selenocystamine, the XPS full spectrum showed a characteristic Se_{3d} peak, and the content of Mg_{1s} and the Auger peak of Mg decreased significantly, verifying that selenocystamine was successfully immobilized on the surface. The N_{1s} peak of Mg-NO can be decomposed into 409.78 eV (NH_x group), 404.78 eV (-N-C=O), and 399.53 eV (C-N), respectively. The peaks at 50.46 eV and 49.62 eV in the Se_{3d} spectrum may be the $3d_{3/2}$ and $3d_{5/2}$ of the Se-Se bond, respectively [28]. It was worth mentioning that the S element was almost undetectable on the Mg-NO surface due to the lack of the S element in selenocystamine and the covering effect of the new coating.

The SEM images of the surface morphologies of the varying specimens are shown in Fig. 3. The surface of the unmodified Mg alloy had obvious scratches caused by polishing. The surface roughness of Mg-OH and Mg-DAM was lessened, and the surface became smoother. Due to the addition of acrylamide during the self-polymerization of dopamine, there were no particle agglomerations on the surface PDA layer. After the photopolymerization of SBMA/2AAM hydrogel, a relatively rough polymer coating appeared on the surface, which may be caused by the aggregation of hydrogel polymers on the surface. After immobilizing bivalirudin on Mg-SBMA/2AAM through amide coupling, the surface morphology showed a few granular particles (Mg-BV), and the aggregation of hydrogel polymers was significantly enhanced, leading to a further reduction in surface roughness and a significant improvement in coating uniformity. This may be because during the grafting process of bivalirudin, the aqueous solution caused the polymer chains of the SBMA/2AAM coating to stretch, it reacted with bivalirudin after absorbing water on the surface, which changed the spatial structure of the surface polymers to some extent, making the coating more uniform and denser. After grafting selenocystamine, small white particles appeared on the surface. This was due to the further crosslinking of EDC on the coating during the grafting process, making the coating denser and rougher.

3.2. In vitro electrochemical corrosion and degradation behaviors

Fig. 4 A-C shows the PDP, EIS, and Bode plots of the varying specimens, and Table 2 illustrates the data of E_{corr}, I_{corr}, and the annual corrosion rate. The values obtained by fitting the EIS curve using the $R_s(Q_{dl}R_{ct})$ equivalent circuit are exhibited in Table 3. The unmodified Mg alloy was prone to corrosion in physiological environments due to its excellent chemical activity, so its E_{corr} was the lowest (−1.47 V) and R_{ct} was the smallest (2454 Ω cm^2), moreover, it had the lowest impedance in the low-frequency region, indicating that the unmodified magnesium alloy had the greatest corrosion tendency. Therefore, among all materials, its I_{corr} (1.31×10^{-5} A cm^{-2}) and d (2.97×10^{-1} mm/y) were the largest, suggesting that it had the fastest corrosion rate and the worst corrosion-resisting properties. Alkaline heat treatment is a commonly used method to fabricate the conversion coating on the surface of magnesium alloys to enhance anti-corrosion properties [29]. The self-polymerized coating of dopamine and acrylamide could effectively resist the corrosive medium corroding the substrate. Therefore, after NaOH treatment and the preparation of DAM coating, E_{corr} went up to

Table 2
The corrosion parameters of the varying magnesium alloys.

Samples	E_{corr}/V	I_{corr}/A·cm^{-2}	d/(mm/y)
Mg	−1.47	1.31×10^{-5}	2.97×10^{-1}
Mg-OH	−1.36	4.21×10^{-6}	3.61×10^{-2}
Mg-DAM	−0.66	1.38×10^{-6}	3.11×10^{-2}
Mg-SBMA/2AAM	−0.44	8.67×10^{-8}	1.96×10^{-3}
Mg-BV	−0.29	1.32×10^{-8}	2.99×10^{-4}
Mg-NO	−0.20	2.92×10^{-9}	6.60×10^{-5}

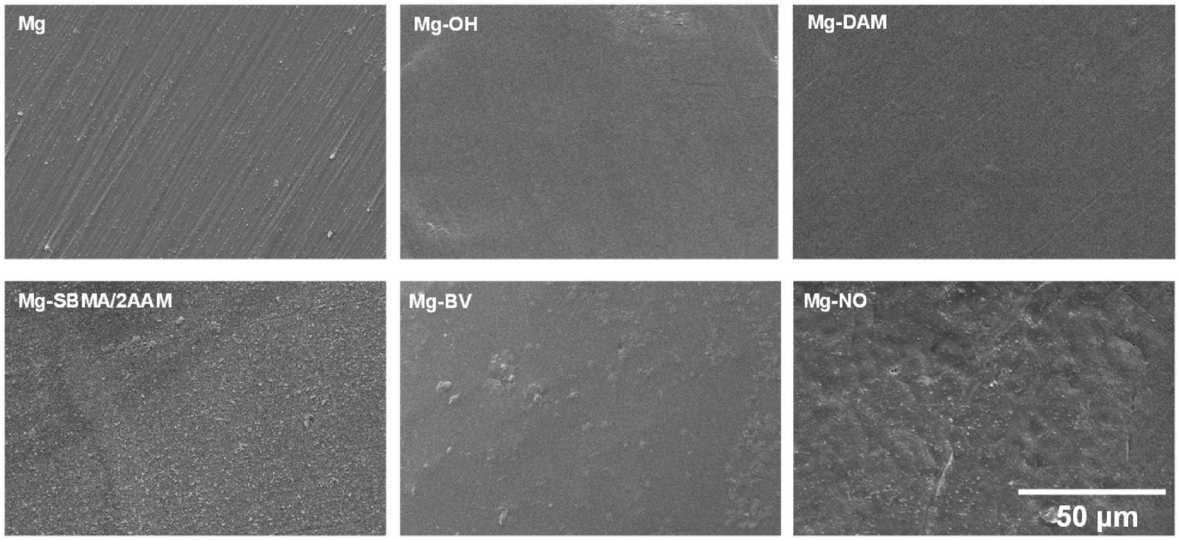

Fig. 3. SEM morphological images of the different specimens.

Table 3
EIS fitting parameters of the varying Mg alloys.

Samples	R_s/(Ω·cm^2)	Q_{dl}/(μF·cm^{-2})	R_{ct}/(Ω·cm^2)
Mg	99.31	1.71×10^{-5}	2454
Mg-OH	92.89	1.16×10^{-5}	4717
Mg-DAM	93.40	9.72×10^{-6}	6365
Mg-SBMA/2AAM	97.63	1.94×10^{-5}	13194
Mg-BV	93.58	1.29×10^{-6}	18186
Mg-NO	97.01	1.54×10^{-5}	24118

Rs, solution resistance; Q_{dl}, double layer capacitance between sample and solution; R_{ct}, the charge transfer resistance.

−1.36 V (Mg-OH) and −0.66 V (Mg-DAM), respectively, and I_{corr} was lowered by an order magnitude in contrast to that of blank Mg alloy, indicating that the corrosion resistance was significantly improved. At the same time, the charge transfer resistance R_{ct} and the impedance of the low-frequency region raised significantly, suggesting that the alkaline heat treatment and DAM coating could augment the corrosion-resisting properties mainly by preventing the charge transfer step of electrochemical reactions. Compared with Mg-DAM, the I_{corr} value of the Mg-SBMA/2AAM sample was lowered by about 16 times and the R_{ct} was increased by about 2 times, suggesting that the anti-corrosion properties of the hydrogel coating modified specimen were further improved. This was mainly because the densely cross-linked hydrogel coating could effectively isolate the corrosion medium from the substrate. In addition, a lot of polar groups (amino, carbonyl, and sulfonic acid groups) in the coating also had a repulsive effect on corrosive anions (such as Cl^-), effectively preventing the migration of corrosive anions and effectively inhibiting charge transfer reaction steps [30], finally improving the corrosion resistance. Therefore, the impedance of the low-frequency region also significantly increased for Mg-SBMA/2AAM. After grafting bivalirudin on Mg-SBMA/2AAM, the E_{corr} of Mg-BV continued to shift positively (−0.30 V), and I_{corr} and d were lowered to 1.32×10^{-8} A cm^{-2} and 2.99 $\times 10^{-4}$ mm/y, indicating a lower corrosion rate and corrosion tendency. Moreover, the curve in the Bode diagram was the highest, which was because the cross-linking effect of EDC on the surface coating during the amidation reaction augmented the compactness of the surface coating (as shown in Fig. 3), effectively slowing down the biodegradation rate of magnesium alloys. After constructing a bioactive coating that could catalyze the NO liberation (Mg-NO), the corrosion potential went up to −0.20 V, while having the smallest I_{corr} (2.92×10^{-9} A cm^{-2}) and the largest R_{ct} (24118 Ω cm^2), implying that the coating had better barrier effect for the rapid corrosion of magnesium alloys. On the one hand, the increase in coating thickness could inhibit anodic dissolution reactions; on the other hand, the completely uniform coverage of the surface coating provided better protection for magnesium alloys, thus strengthening anti-corrosion properties. In addition, the crosslinking effect of EDC on the coating also helped to improve corrosion resistance.

The degradation performance of the different modified Mg alloys was further evaluated using immersion experiments. Generally speaking, magnesium alloys undergo corrosion degradation in aqueous

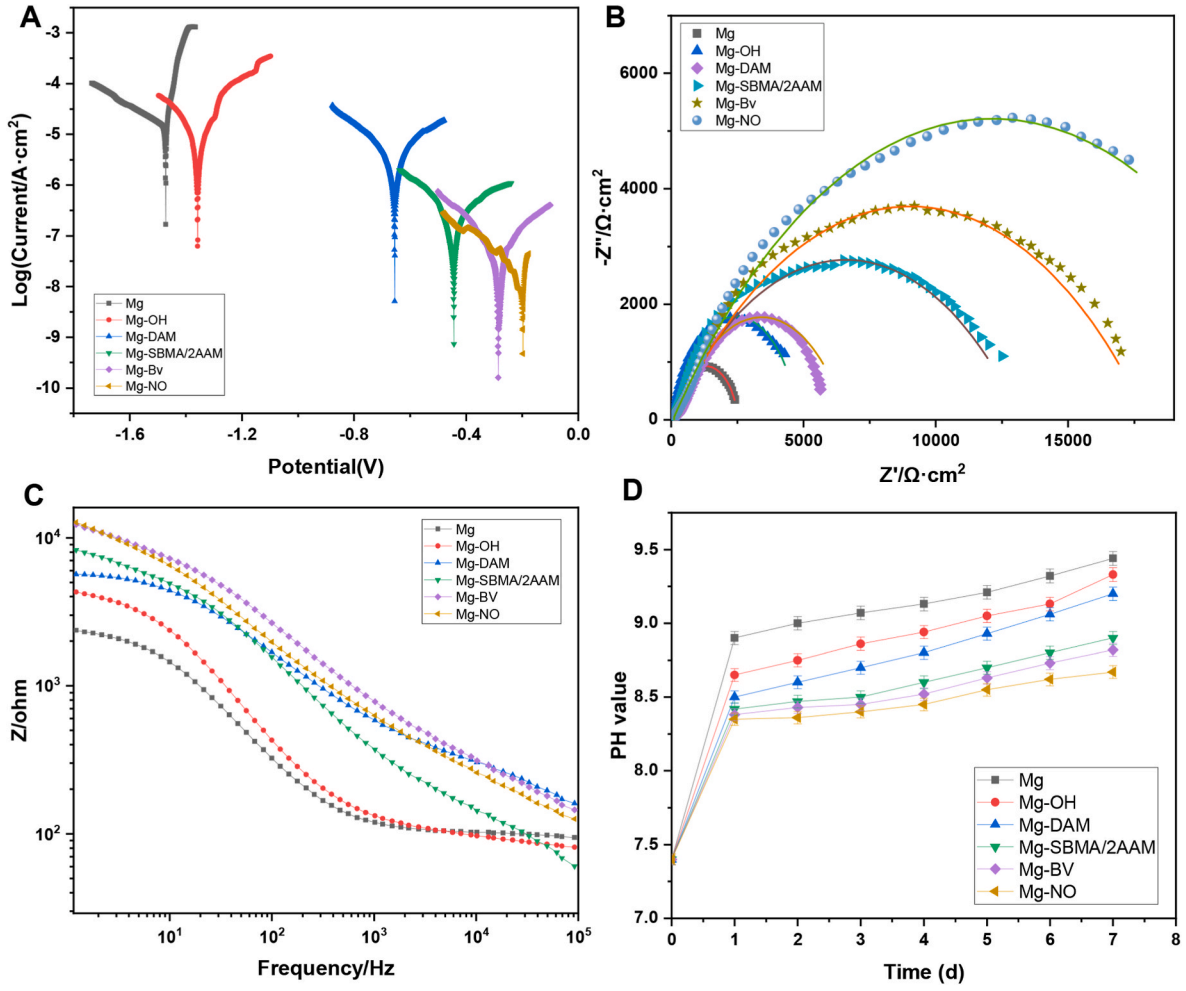

Fig. 4. The polarization curves (A); EIS spectra (B, Line: calculative values; Scatter: original values.) and Bode image (C) of the varying magnesium alloys; (D) pH changes of the solutions for immersing varying magnesium alloys.

corrosive media (such as physiological environments), generating magnesium ions, and decomposing water into hydroxide ions and hydrogen gas. Therefore, measuring the concentration of hydroxide ions (pH value) during the corrosion process can be used to characterize the corrosion degradation behavior of magnesium alloys. Generally speaking, the more magnesium ions are released per unit time, the more hydroxide ions are generated, resulting in varying degrees of pH increase in the corrosive medium. The pH alterations of SBF solutions for varying modified magnesium alloys are illustrated in Fig. 4D, and the corrosion morphologies are displayed in Fig. 5. Combined with the results of Figs. 4D and 5, it could be found that the pH value of the immersion solution for the unmodified Mg alloy was much larger than those of other samples throughout the entire immersion process, suggesting that its corrosion speed was the largest. At the same time, after 1 day of immersion, obvious corrosion cracks appeared on the Mg surface. As the time increased, the corrosion cracks were raised and the dimensions significantly expanded. After 14 days, large cracks and more corrosion by-products could be found, demonstrating that the corrosion resistance of the unmodified Mg alloy was worse than other samples. This was due to the high chemical reactivity of the unmodified Mg alloy, which is extremely prone to degradation, especially in a Cl^- environment [31]. The loose surface oxide layer produced by natural oxidation can form soluble chlorides upon exposure to a corrosive environment containing Cl^-. After alkali heat treatment and preparation of DAM coating, the pH of the immersion medium was lowered (compared to Mg), and no significant corrosion cracks were observed after one day of immersion. However, with the increase in immersion time, the surface coating dissolved slowly due to unstable chemical properties. After 7 d immersion, the pH values reached 9.33° (Mg-OH) and 9.20° (Mg-DAM). After 3 days of immersion, cracks appeared on the Mg-OH surface accompanied by the occurrence of white corrosion products, which was due to the inability of the surface magnesium hydroxide coating to ensure continuous and effective corrosion control in an environment containing chloride ions. Therefore, the $Mg(OH)_2$ passivation coating could only moderately protect the substrate from external aggressive liquid and play a role in resisting acute corrosion [32]. After soaking for 3 days, Mg-DAM also began to corrode, indicating that the DAM coating may dissolve, which may be due to the loss of the DAM

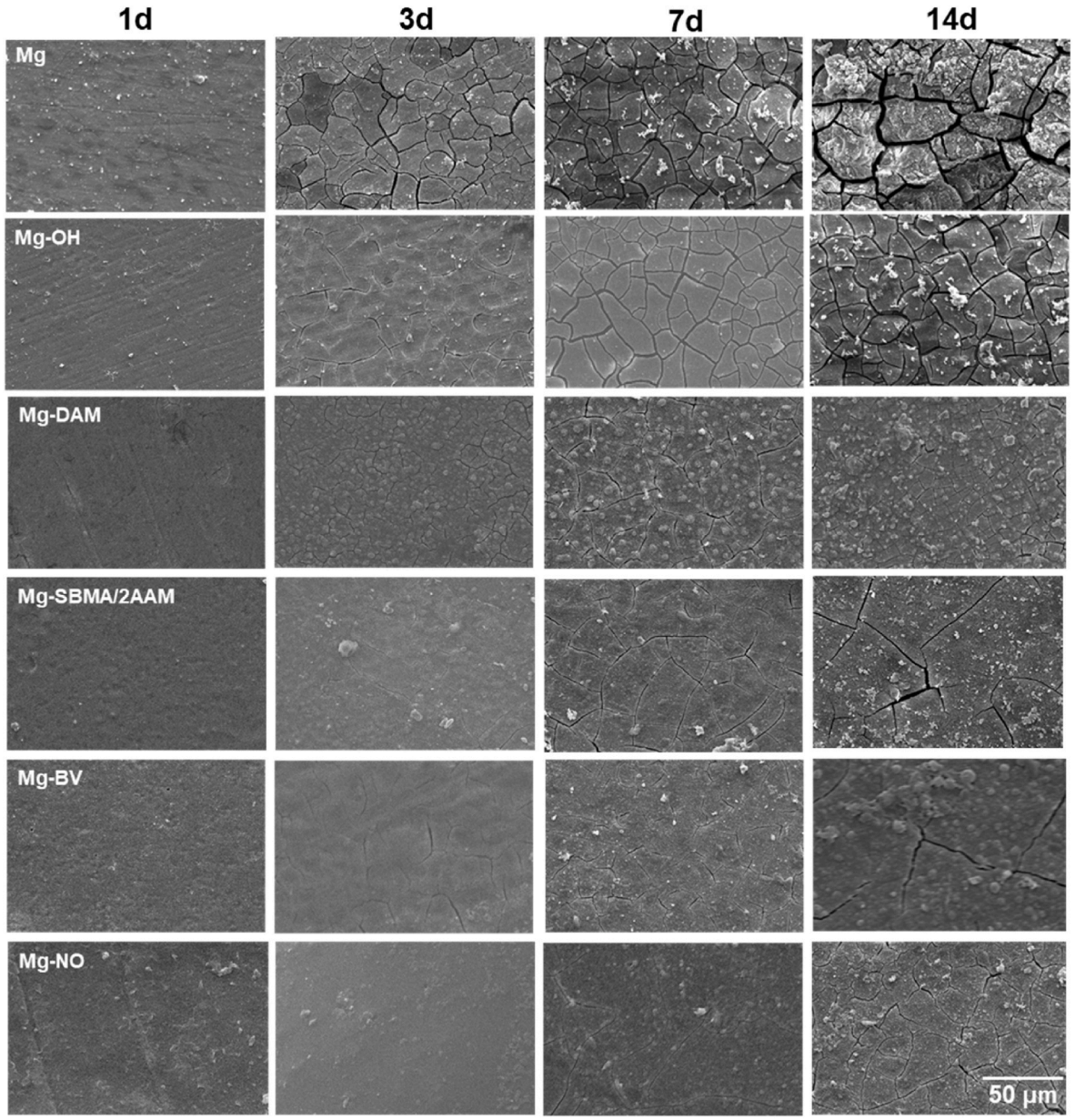

Fig. 5. SEM images of the varying magnesium alloys immersed in SBF for different times.

coating due to corrosion reactions and Mg^{2+} pitting at the metal-hydroxide interface [19]. After photopolymerization treatment, the pH value of Mg-SBMA/2AAM decreased more (compared to Mg), which was due to the high crosslinking density of the hydrogel, resulting in strong binding force of the coating with the substrate, effectively slowing down the corrosion rate. Meanwhile, it could also be observed from the SEM images that the cracks could only be found on the Mg-SBMA/2AAM surface after 7 days, however, the crack width was small and the coating remained intact, manifesting that the protective effect of the surface coating was slowly reduced. After grafting bivalirudin, the pH value increased gently in the first 3 days, suggesting that the better coating compactness effectively resisted the corrosion of erosive ions. After 3 days of immersion, the pH value rapidly increased, which may indicate that the coating was corroded. For Mg-NO, the pH value tended to be flat, suggesting that the corrosion speed of Mg-NO was the slowest. This was because the increase in coating thickness offered long-lasting effective protection for the substrate, consistent with the results of electrochemical experiments. From Fig. 5, it can be found that the surfaces of Mg-BV and Mg-NO only showed slight corrosion cracks after being immersed for 7 days, verifying that the surface coating had good anti-corrosion properties and it could act as a shielding layer to prevent the penetration of aqueous solutions and aggressive ions into the metal surface, thus delaying degradation. After soaking for 14 days, the Mg-NO sample showed the slowest corrosion, with only a few corrosion by-products produced, consistent with the electrochemical results (Fig. 4A). After soaking for 14 days, there was no significant degradation, and the relatively intact coating remained, possibly due to the increased coating thickness providing good insulation against corrosive media.

3.3. Surface wettability and protein adsorption behaviors

When a biomaterial is implanted into the human body, the first event that occurs is protein adsorption on the surface [33]. Albumin and fibrinogen are two important proteins in the blood. Generally speaking, the adsorption of albumin on the surface can improve blood compatibility, while the adsorption of fibrinogen on the surface can lead to poor anticoagulant performance. In addition, as is well known, human tissues contain a large amount of water; therefore, the surface wettability of biomaterials has a significant impact on their biocompatibility. For blood-contact biomaterials, hydrophilic surfaces have better wettability and can form hydration layers on the surface, which to some extent prevent non-specific protein adhesion and platelet adhesion. At the same time, hydrophilic surfaces are also conducive to the adsorption of albumin in plasma, thereby improving the anticoagulant performance of the biomaterial. The surface wettability goes hand in hand with the protein adsorption behavior on the material surface [34], significantly influencing blood compatibility and EC growth. This study applied the WCA to examine the surface wettability of different modified samples. The BCA assay was carried out to investigate the adsorption behaviors of two important plasma proteins (albumin and fibrinogen) on different Mg alloy surfaces. The results are illustrated in Fig. 6. Compared to the unmodified Mg alloy, the WCA of Mg-OH was lowered from 69.7° to 40.1°, suggesting that the NaOH treatment increased the surface hydrophilicity. Because albumin is more easily adsorbed on hydrophilic surfaces, and fibrinogen adsorption occurs more easily on hydrophobic surfaces [35], there was a growth in BSA adsorption and a decrease in Fib adsorption on the Mg-OH surface. In the process of dopamine self-polymerization, the catechol group of PDA can covalently link with the amine groups of acrylamide through the Michael addition reaction and Schiff base reaction, which may lower the non-covalent forces between PDA molecules and further enhance the hydrophilicity. For this reason, the WCA of Mg-DAM continued to decrease to 26.4°, leading to a reduction in the Fib adsorption (26.8 μg/cm^2). Hydrogel coating generally has an excellent ability to absorb water molecules, so most hydrogels have good hydrophilicity. Therefore, after surface photopolymerization to fabricate the SBMA/2AAM hydrogel coating, the surface hydrophilicity was further enhanced, and the WCA was lowered to 18.1°, which led to a significant increase in BSA adsorption. On the one hand, the charged groups in the hydrogel coating could form a stable hydration layer by combining water molecules through electrostatic forces, which exhibit a strong repulsive force on proteins near the modified surface, hindering protein adsorption [36]. On the other hand, the adsorbed albumin can play a good shielding role in inhibiting the transmission of soluble substances and corrosive ions to some degree [37], thus improving corrosion resistance and albumin adsorption. As a polypeptide anticoagulant, bivalirudin has a lot of hydrophilic groups, such as carboxyl (-COOH) and hydroxyl (-OH) groups in its molecule. Therefore, further grafting bivalirudin onto the hydrogel coating surface should improve its hydrophilicity. However, due to the cross-linking effect of EDC on the coating during the grafting of bivalirudin, the change in surface water contact angle was not significant. Compared with Mg-SBMA/2AAM, although the hydrophilicity changed slightly, the albumin adsorption increased significantly, and the fibrinogen adsorption decreased, which was due to the strong inhibitory effect of bivalirudin on fibrinogen adsorption [38]. Moreover, bivalirudin and fibrinogen have the same charge, and this electrostatic repulsion also prevents fibrinogen adsorption [39]. After further immobilization of selenocystamine (Mg-NO), the water contact angle decreased to 11.0°, and the surface wettability approached the super hydrophilicity, with the highest albumin adsorption on the surface. It was considered that the existence of surface hydrophilic amine groups and the increase in roughness could further enhance the surface hydrophilicity and thus promote albumin adsorption. However, it was worth noting that no significant change in fibrinogen adsorption could be found compared to the Mg-BV.

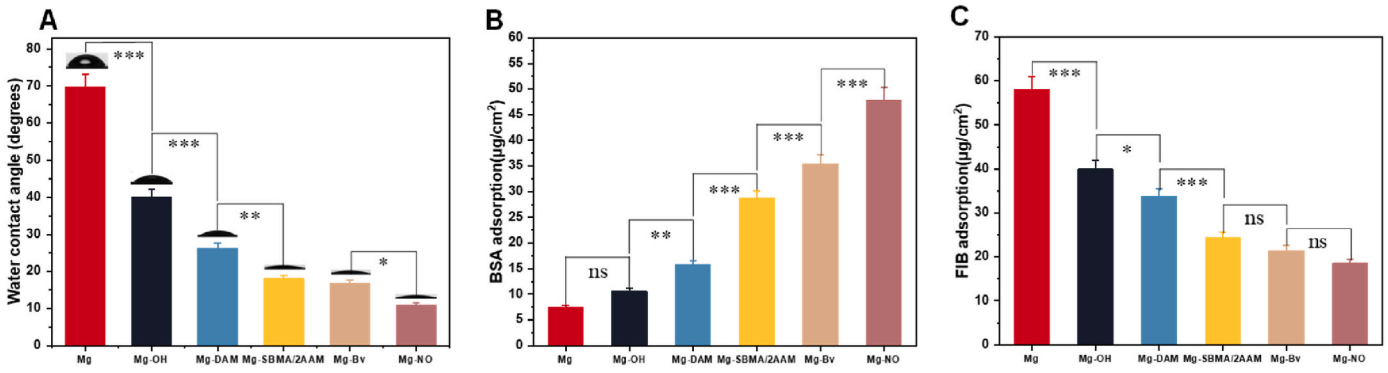

Fig. 6. Water contact angles (A), BSA (B), and Fib (C) adsorption amount on varying magnesium alloys. Data were obtained from three parallel specimens and expressed as mean value ± SD (n = 3), *p < 0.05, **p < 0.01, ***p < 0.001, ns, no significance.

3.4. Catalytic release behavior of NO

Selenocystamine (SeCA) has a GPx-like catalytic activity, it can catalytically decompose RSNO to generate NO gas using GSH as a reducing agent [40]. The reaction mechanism is $RSe-SeR+2R'SNO\xrightarrow{GSH}2RSe-R'+2NO$. The Griess reagent method was applied to characterize the behavior of in vitro NO-generation, and the results are illustrated in Fig. 7. As is evident from Fig. 7, both materials with and without reducing agents (Mg-NO-C and Mg-NO) could continue to liberate NO in the presence of NO donor (GSNO). In the case of the existence of reducing agents (GSH), the NO concentration of Mg-NO-C significantly increased, indicating the important role of GSH in the catalytic release of NO. Meanwhile, as shown in Fig. 7, NO in both cases had a burst release period, which was related to the change in the donor concentration of the solution and the presence of surface catalysts. The initial solution had a high concentration of NO donor, resulting in a rapid NO release, thus exhibiting a significant burst release phenomenon. The burst release without the reducing agent was significantly smaller than that of the presence of GSH. However, in the absence of the reducing agent, there was a burst NO release, it was related to the natural decomposition of the GSNO donor and the catalytic effect of the surface selenocystamine. Selenocystamine still had a certain catalytic effect on the NO release without the reducing agent. In both cases of NO release, after the burst release period of NO, the NO release tended to stabilize. This was because as the time increased, the NO donor concentration continuously decreased, giving rise to a decrease in the NO release through catalytic reaction, thus slowing down the release rate.

3.5. Anticoagulant properties

Fig. 8 A-D displays the morphologies of the attached platelets (A), platelet number (B), GMP-140 (C), and hemolysis rate (D) of the varying surfaces. It was evident that, owing to the inferior bioactivity of the Mg surface, many platelets adhered to the surface, showing a serious aggregation state with many pseudopodia, suggesting that many platelets were activated. The outcomes of the GMP140 assay also verified that the platelet activation on the unmodified Mg alloy was the largest among all samples. In addition, the hemolysis rate of the Mg alloy was as high as 57.3 %, which was because the release of Mg^{2+} and OH^- resulted from the fast corrosion of unmodified Mg alloy improved pH value and magnesium ion concentration, which increased the osmotic pressure difference between the two sides of the membrane of red blood cell (RBC), resulting in RBC rupture and thus serious hemolysis. After alkali-heat treatment and the fabrication of the DAM layer, the two modified layers improved the corrosion-resisting properties to some degree, reducing the negative impact of corrosion products on blood compatibility. As a result, the attached platelets on these surfaces gradually decreased, but the GMP140 concentration remained high, indicating high platelet activation. Although the hemolysis rates of Mg-DAM and Mg-OH decreased significantly, they still did not meet national standards (<5 %), suggesting that blood compatibility needed to be improved. Due to the unique 3D network structure of the hydrogel coating, it could capture a lot of water molecules, thereby simulating the ECM structure. Upon contact with blood, it can lower the frictional stimulation on RBCs. The fabrication of the surface hydrogel coating further enhanced the corrosion-resisting properties of the Mg alloy. During the hemolysis experiment, it almost did not cause corrosion degradation. Therefore, the hemolysis value of Mg-SBMA/2AAM was reduced to 4.86 %, satisfying relevant national standards (<5 %). In addition, the hydrogel coating has good surface wettability, and it can effectively prevent fibrinogen adsorption in the plasma, thereby reducing the risk of thrombosis and augmenting hemocompatibility. Therefore, the adhesion of platelets and the GMP140 expression on the Mg-SBMA/2AAM sample were lowered significantly, indicating that the coating had good anticoagulant properties. Bivalirudin is a potent, highly specific, and reversible thrombin inhibitor that not only inhibits the proliferation of smooth muscle cells, allowing the inner layer of endothelial cells to recover; but also inhibits thrombin-mediated platelet activation and aggregation [41], thus improving the hemocompatibility. Unlike heparin, bivalirudin blocks thrombin without cofactors like antithrombin III and does not activate platelets [42], making it an ideal alternative to heparin. At the same time, bivalirudin can strongly inhibit FIB adsorption through the antithrombin pathway [43], which also contributes to better hemocompatibility. As shown in Fig. 8, it could be observed that grafting bivalirudin on the SBMA/2AAM hydrogel coating could further significantly inhibit platelet adhesion and GMP140 expression. Most platelets adhering to the surface remained spherical because bivalirudin could directly inhibit thrombin through specific binding to anionic exosomes, clot, and catalytic sites of circulating thrombin, thereby reducing platelet adhesion and activation. In the meantime, the hemolysis rate of Mg-BV was lessened to 4.07 %, proving that the immobilization of bivalirudin on the surface significantly improved its anticoagulant properties. It has been demonstrated that selenocystamine can exhibit catalytic activity similar to glutathione peroxidase (GPx) [44], and induce an increase in cGMP to impede platelet adhesion. Meanwhile, a small amount of NO donor in the blood would also be catalyzed by the surface selenocystamine to release NO, which also had a certain inhibitory action on platelet adhesion and activation. Therefore, after further grafting selenocystamine, the platelet adhesion and activation were significantly lowered, and at the same time, the hemolysis continued to decrease (3.55 %). On the one hand, the improved anti-corrosion properties (Fig. 4) can resist the contact of corrosive media with the substrate surface, providing better protection. On the other hand, the surface wettability (Fig. 6A) endowed the coating with a good effect of preventing nonspecific adhesion of platelets and RBCs, improving blood compatibility. As an effective gas signaling molecule that inhibits platelet adhesion and activation, NO can inhibit thromboxane A2 receptors through the phosphorylation of cGMP-dependent protein kinases, thereby inhibiting platelet aggregation and activation. NO can act with RBCs by binding with the heme portion of hemoglobin, forming S-nitrosylhemoglobin and giving rise to the formation of methemoglobin [45]. Therefore, after adding the reducing agent (GSH) and NO donor (GSNO), only a few round and inactive platelets were observed on Mg-NO-C, with a hemolysis rate of only 3.13 %, unveiling that the catalytic release of NO can maintain good bioactivity and further improve the blood compatibility.

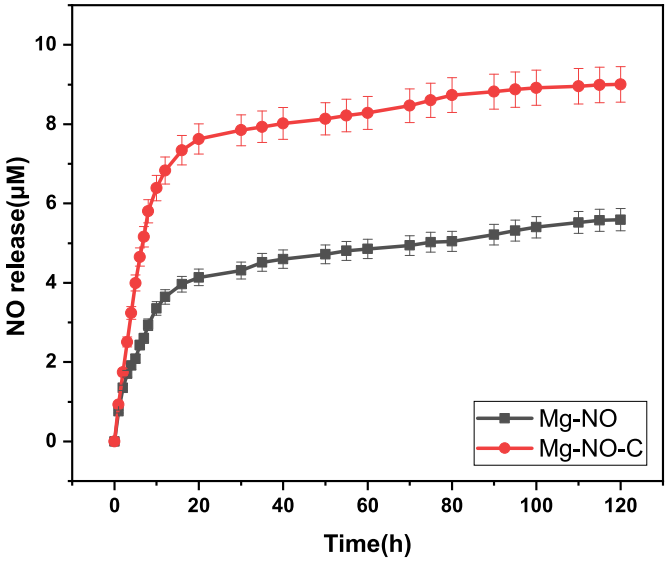

Fig. 7. The NO liberation curves of Mg-NO and Mg-NO-C.

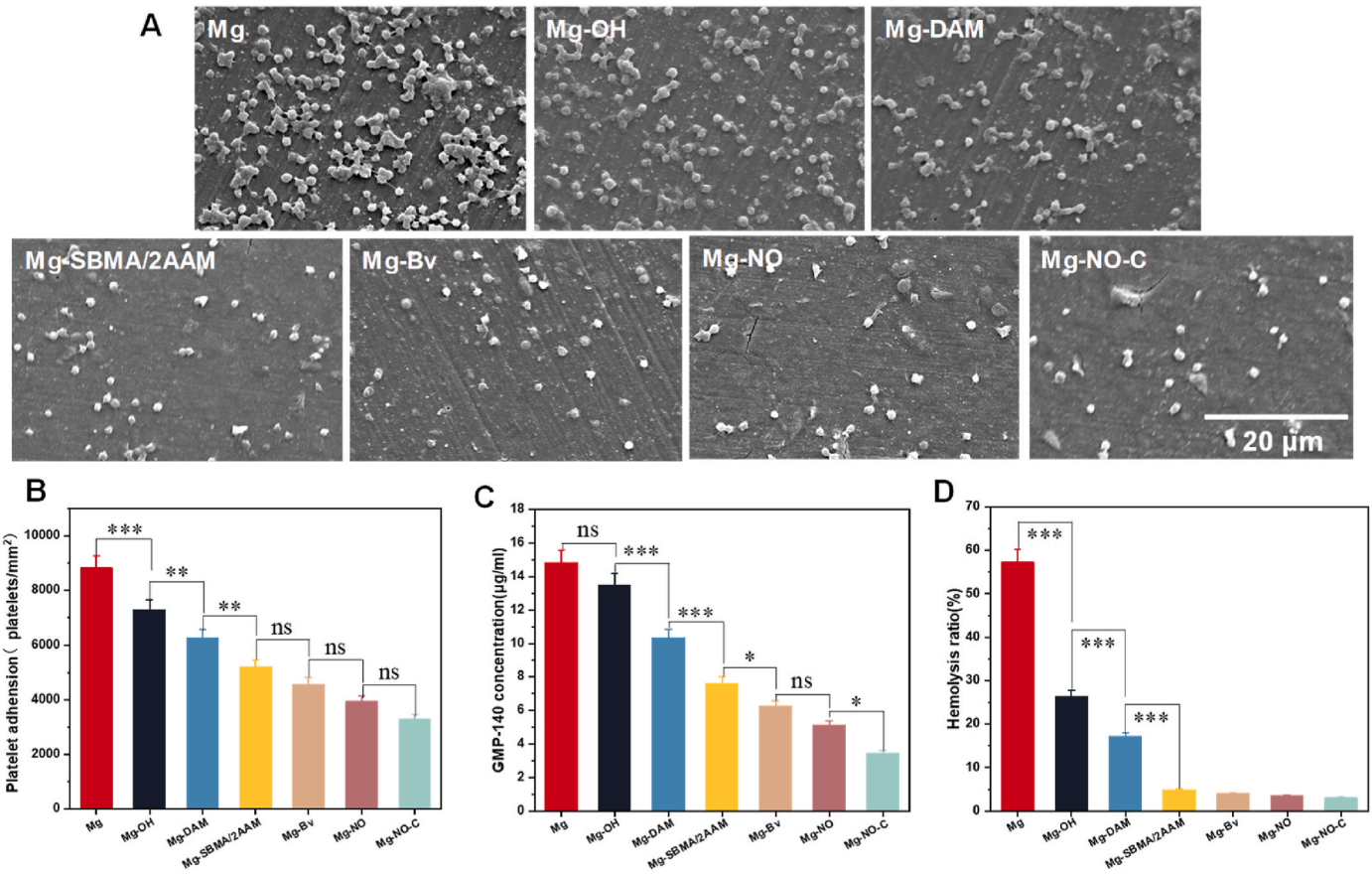

Fig. 8. Morphologies of the attached platelets (A), the number of platelets (B), GMP-140 concentration (C), and hemolysis rate (D) for the varying magnesium alloys. Three parallel samples were examined for platelet number, GMP-140, and hemolysis rate; Data were expressed as mean ± SD (n = 3), *p < 0.05, **p < 0.01, ***p < 0.001, ns, no significance.

3.6. EC growth behaviors

Fig. 9A shows the images of the adhered ECs on varying surfaces at different times. Fig. 9 B, C, and D exhibit the outcomes of CCK-8, VEGF, and NO assays, respectively. Generally speaking, cells attached to the biomaterial surface with a spreading state indicate better cell migration and growth performance. As shown in Fig. 9A, cells on the surfaces of Mg, Mg-OH, and Mg-DAM exhibit a wrinkled circular shape, indicating weaker spreading and migration ability and thus representing suboptimal cell growth. The adherent cells on the unmodified Mg alloy were the lowest and displayed an inferior spreading state, and no significant increase could be found after 24 h culture. It was considered that the rapid magnesium degradation led to a highly alkaline environment and high concentrations of Mg^{2+}, and the surface of the pristine Mg alloy lacked cell adhesion sites, making it difficult for ECs to survive on the surface. The adhered cells also had difficulty in expressing VEGF and NO, resulting in the lowest expression levels of VEGF (23.2 ng/L) and NO (1.2 μM/L). The attached cells increased slightly on Mg-OH and Mg-DAM, it was considered that the increase in surface hydrophilicity and the PDA layer could facilitate the EC growth to a certain extent, which was also beneficial to the upregulation of VEGF and NO expression. However, the increase in cell quantity was not significant and the cell morphologies also exhibited wrinkled circular shape without pseudopods, indicating its spreading ability did not ameliorate obviously. After the fabrication of the hydrogel coating through photopolymerization, the cells significantly increased, the cell morphology began to spread, and the CCK-8 value was also increased, showing improved cell growth. The expression levels of VEGF and NO for Mg-SBMA/2AAM also further increased (118.4 ng/L for VEGF and 6.2 μM/L for NO), which could be due to the electrostatic interaction between amine groups and cell membranes, they have opposite charges. The structure of the hydrogel similar to the ECM and suitable mechanical properties were also important factors in promoting cell growth. At the same time, the various active groups on the surface were helpful for the adsorption and activity maintenance of adhesive proteins, which could enhance the growth and functional expression of ECs. Yang et al. [26] reported that grafting bivalirudin on the plasma-polymerized polyacrylamide surface could enhance EC adhesion, proliferation, and migration, and inhibit thrombosis by rapidly promoting the formation of surface endothelium *in vivo*. After bivalirudin was immobilized on the hydrogel coating surface, the cell adhesion and proliferation were further improved, with the cells showing a spread-out state and exhibiting better cell migration ability. At the same time, the expression of VEGF and NO (198.6 ng/L and 6.1 μM/L) in the cells adhering to the surface also further increased, suggesting that the coating offered a favorable microenvironment for EC adhesion and migration, thereby promoting the growth and normal functional expression of ECs. Organic selenium can produce superoxide through glutathione oxidation or nitrite, both are beneficial in inhibiting intimal hyperplasia [46]. After further grafting selenocystamine on the Mg-BV surface, the CCK-8 value was further augmented, suggesting a high number of cell adhesion and proliferation. It was considered that the coating significantly enhanced the corrosion-resisting properties while imparting good bioactivity to magnesium alloys, promoting EC proliferation and differentiation. Meanwhile, as exhibited in Fig. 9, the expression of VEGF and NO on the Mg-BV surface decreased slightly after 24 h (196.3 ng/L and 5.3 μM/L). On the one hand, it may be due to the excellent hydrophilicity of the Mg-NO surface, which affected cell adhesion and inhibited the functional expression of ECs. On the other

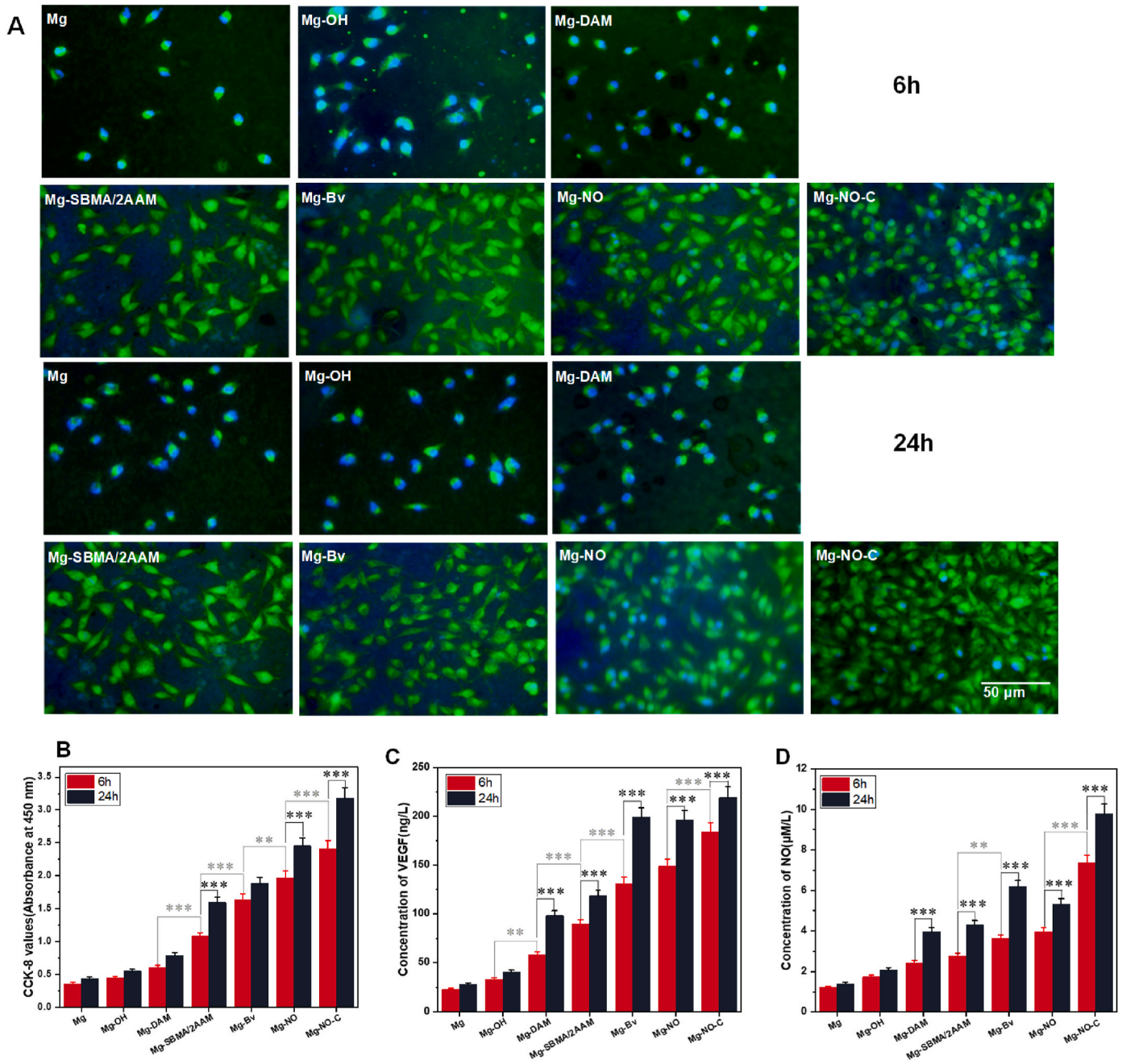

Fig. 9. (A) The fluorescent images of the endothelial cells attached to the different magnesium alloy surfaces for 6 h and 24 h, respectively. (B) CCK-8 values, (C) VEGF, and (D) NO expression of the endothelial cells adhered on the varying magnesium alloy surfaces, five parallel samples were characterized and data were expressed as mean ± SD (n = 5), *p < 0.05, **p < 0.01, ***p < 0.001.

hand, the grafting of selenocystamine onto the surface could reduce the activity of bivalirudin. NO has been proven to be a gas-signaling molecule that can effectively enhance EC adhesion and growth. NO can regulate biological processes through its high reactivity and the ability to bind with heme iron to activate guanylate cyclase (sGC), which produces cyclic guanosine monophosphate (cGMP) to bind with phosphodiesterase or cGMP-dependent protein kinase (PKG) and thus induces a series of events that promote various biological processes, such as inhibiting platelet aggregation and promoting EC growth [47]. In addition, NO can also inhibit monocyte adhesion and EC apoptosis [48]. Therefore, after adding NO donor and reducing agent, the CCK-8 data of Mg-NO-C was expanded significantly after 24 h, indicating that the continuous NO release induced ECs to secrete more ECM proteins, further facilitating EC growth. In addition, in the case of catalytic NO-generation, the expression levels of NO and VEGF rapidly increased to 219 ng/L and 9.7 μM/L, respectively, indicating that NO provided a microenvironment friendly to ECs, significantly enhancing the functional expression of VEGF and NO in ECs, thereby facilitating rapid regeneration of the endothelium.

4. Conclusion

The hydrogel coating with excellent hydrophilicity was successfully fabricated on the magnesium alloy surface using UV photopolymerization of SBMA and acrylamide, and bivalirudin and selenocystamine were grafted on this hydrogel coating, thus constructing a hydrogel coating with excellent hemocompatibility and catalytic release of NO to promote EC growth. Compared to the unmodified Mg alloy, the

hydrophilicity of the surface-modified Mg alloy was significantly enhanced, with the ability to adsorb BSA preferentially and enhanced anti-corrosion properties. Meanwhile, surface grafting of bivalirudin and selenocystamine not only ameliorated the blood compatibility, including inhibiting platelet adhesion and activation, and reducing hemolysis rate, but also effectively facilitated the adhesion, proliferation, and VEGF and NO expressions of ECs. In the catalytic release of NO, the hemocompatibility, EC growth, and EC functional expression were further enhanced. Consequently, the research in this study could be applied to modify the surface of magnesium alloy vascular stent materials to augment the corrosion-resisting properties, anticoagulant properties, and ability to facilitate vascular endothelial regeneration, promoting the research and application of magnesium-based alloy intravascular stents.

CRediT authorship contribution statement

Changjiang Pan: Writing – original draft, Supervision, Project administration, Funding acquisition, Conceptualization. **Naiquan Yang:** Writing – original draft, Supervision, Methodology, Data curation. **Jie Chen:** Writing – review & editing, Visualization, Methodology, Investigation. **Qiuyang Zhang:** Writing – review & editing, Visualization, Validation. **Linhong Deng:** Writing – review & editing. **Teng Luo:** Writing – review & editing. **Lingjie Meng:** Writing – review & editing, Investigation.

Declaration of competing interest

The authors declare that they have no known competing financial interests or personal relationships that could have appeared to influence the work reported in this paper.

Acknowledgments

This work was financially supported by the Natural Science Foundation of Jiangsu Province (BK20241941), the National Natural Science Foundation of China (31870952), and the Key Program or Natural Science Foundation of Jiangsu Higher Education Institutions of China (23KJA430004).

Data availability

Data will be made available on request.

References

[1] S.K. Guan, D. Mei, J.F. Wang, Z.Q. Zhang, P.H. Du, L.C. Bai, C. Yan, J.A. Li, J. Wang, S.J. Zhu, Mg alloy cardio-/cerebrovascular scaffolds: developments and prospects, J. Magnesium Alloys 11 (2023) 4011–4042.
[2] C.J. Pan, X.H. Liu, Q.X. Hong, J. Chen, Y.X. Cheng, Q.Y. Zhang, L.J. Meng, J. Dai, Z. M. Yang, L.R. Wang, Recent advances in surface endothelialization of the magnesium alloy stent materials, J. Magnesium Alloys 11 (2023) 48–77.
[3] P. Tong, L. Chen, X. Sun, H. Li, Y. Feng, J. Li, S. Guan, Surface modification of biodegradable magnesium alloy with poly (L-lactic acid) and sulfonated hyaluronic acid nanoparticles for cardiovascular application, Int. J. Biol. Macromol. 237 (2023) 124191.
[4] K.P. Liu, A.Y. Cheng, J.L. You, Y.H. Chang, C.C. Tseng, M.D. Ger, Biocompatibility and corrosion resistance of drug coatings with different polymers for magnesium alloy cardiovascular stents, Colloids Surf., B 245 (2024) 114202.
[5] Z. Hou, M. Xiang, N. Chen, X. Cai, B. Zhang, R. Luo, L. Yang, X. Ma, L. Zhou, F. He, H. Yu, Y. Wang, The biological responses and mechanisms of endothelial cells to magnesium alloy, Regen Biomater 8 (2021) rbab017.
[6] M. Echeverry-Rendón, F. Echeverria, H. Buikema, M.C. Harmsen, G. Krenning, Endothelial function after the exposition of magnesium degradation products, Biomater. Adv. 134 (2022) 112693.
[7] L. Meng, X. Liu, L. Liu, Q. Hong, Y. Cheng, F. Gao, J. Chen, Q. Zhang, C. Pan, Comparative investigation of the corrosion behavior and biocompatibility of the different chemical conversion coatings on the magnesium alloy surfaces, Metals 12 (2022) 1644.
[8] M. Guo, L. Cao, P. Lu, Y. Liu, X. Xu, Anticorrosion and cytocompatibility behavior of MAO/PLLA modified magnesium alloy WE42, J. Mater. Sci. Mater. Med. 22 (2011) 1735–1740.
[9] Z.Q. Zhang, Y.X. Yang, J.A. Li, R.C. Zeng, S.K. Guan, Advances in coatings on magnesium alloys for cardiovascular stents - a review, Bioact. Mater. 6 (2021) 4729–4757.
[10] Y. Wang, Y. Zhao, X. Wang, Y. Xie, L. Bai, S. Guan, Fucoidan/collagen composite coating on magnesium alloy for better corrosion resistance and pro-endothelialization potential, Int. J. Biol. Macromol. 255 (2024) 128044.
[11] Y.L. Lai, C.R. Lin, C.C. Yen, S.K. Yen, Heparin-loaded composite coatings on porous stent from pure magnesium for biomedical applications, J. Funct. Biomater. 14 (2023) 519.
[12] L. Wang, R. Xu, L. Meng, Q. Zhang, Z. Qian, J. Chen, C. Pan, A fucoidan-loaded hydrogel coating for enhancing corrosion resistance, hemocompatibility and endothelial cell growth of magnesium alloy for cardiovascular stents, Biomater. Adv. 163 (2024) 213960.
[13] Y. Wu, L. Chang, J. Li, L. Wang, S. Guan, Conjugating heparin, Arg-Glu-Asp-Val peptide, and anti-CD34 to the silanic Mg-Zn-Y-Nd alloy for better endothelialization, J. Biomater. Appl. 35 (2020) 158–168.
[14] M. Ali, M. Elsherif, A.E. Salih, A. Ul-Hamid, M.A. Hussein, S. Park, A.K. Yetisen, H. Butt, Surface modification and cytotoxicity of Mg-based bio-alloys: an overview of recent advances, J. Alloys Compd. 825 (2020) 154140.
[15] Z. Xu, G. Liu, P. Liu, Y. Hu, Y. Chen, Y. Fang, G. Sun, H. Huang, J. Wu, Hyaluronic acid-based glucose-responsive antioxidant hydrogel platform for enhanced diabetic wound repair, Acta Biomater. 147 (2022) 147–157.
[16] A.S. Mikhail, R. Morhard, M. Mauda-Havakuk, M. Kassin, A. Arrichiello, B. J. Wood, Hydrogel drug delivery systems for minimally invasive local immunotherapy of cancer, Adv. Drug Deliv. Rev. 202 (2023) 115083.
[17] L. Lu, S. Yuan, J. Wang, Y. Shen, S. Deng, L. Xie, Q. Yang, The formation mechanism of hydrogels, Curr. Stem Cell Res. Ther. 13 (2018) 490–496.
[18] C. Pan, C. Zuo, J. Chen, Q. Zhang, L. Deng, Y. Liu, P. Ding, Constructing sodium alginate/carboxymethyl chitosan coating capable of catalytically releasing NO or CO for improving the hemocompatibility and endothelialization of magnesium alloys, Int. J. Biol. Macromol. 279 (2024) 135166.
[19] L. Faxälv, T. Ekblad, B. Liedberg, T.L. Lindahl, Blood compatibility of photografted hydrogel coatings, Acta Biomater. 6 (2010) 2599–2608.
[20] Y. Chen, H. Qian, X. Wang X, P. Liu, G. Yuan, L. Huang, J. Yi, To improve corrosion resistance and hemocompatibility of magnesium alloy via cathodic plasma electrolytic deposition combined with surface thiol-ene photopolymerization, Mater. Lett. 158 (2015) 178–181.
[21] H.R. Bakhsheshi-Rad, E. Hamzah, M. Daroonparvar, S.N. Saud, M.R. Abdul-Kadir, Bi-layer nano-TiO_2/FHA composite coatings on Mg–Zn–Ce alloy prepared by combined physical vapour deposition and electrochemical deposition methods, Vacuum 110 (2014) 127–135.
[22] Y. Ji, C. Zuo, J. Chen, Q. Zhang, Y. Sun, Q. Xiong, C. Pan, Constructing a catalytical NO-generation coating on a polyurethane surface to enhance hemocompatibility and promote endothelial cell growth, Sur. Interfaces 52 (2024) 104985.
[23] Q. Zhang, L. Zhang, M. Yang, Q. Hong, Z. Yang, S. Liu, Q. Xiong, C. Pan, Construction of Chi(Zn/BMP2)/HA composite coating on AZ31B magnesium alloy surface to improve the corrosion resistance and biocompatibility, Nanotechnol. Rev. 10 (2021) 870–882.
[24] C.C. Ho, S.J. Ding, Structure, properties and applications of mussel-inspired polydopamine, J. Biomed. Nanotechnol. 10 (2014) 3063–3084.
[25] N. Huang, S. Zhang, L. Yang, M. Liu, H. Li, Y. Zhang, S. Yao, Multifunctional electrochemical platforms based on the michael addition/schiff base reaction of polydopamine modified reduced graphene oxide: construction and application, ACS Appl. Mater. Interfaces 7 (2015) 17935–17946.
[26] Z. Yang, Q. Tu, M.F. Maitz, S. Zhou, J. Wang, N. Huang, Direct thrombin inhibitor-bivalirudin functionalized plasma polymerized allylamine coating for improved biocompatibility of vascular devices, Biomaterials 33 (2012) 7959–7971.
[27] C.Y. Liu, C.J. Huang, Functionalization of polydopamine via the aza-michael reaction for antimicrobial interfaces, Langmuir 32 (2016) 5019–5028.
[28] S. Liu, X. Liu, M. Chen, D. Wang, X. Ge, W. Zhang, X. Wang, C. Wang, T. Qin, H. Qin, L. Qiao, D. Zhang, X. Ou, W. Zheng, High-density/efficient surface active sites on modified separators to boost Li-S batteries via atomic Co^{3+}-Se termination, Nano Res. 15 (2022) 7199–7208.
[29] J.Y. Zhu, C.X. Jia, Y.Z. Duan, Study on corrosion resistance of alkali-heat modified magnesium alloy surface, Met. Mater. Int. 29 (2023) 1638–1651.
[30] H. Wang, W. Liu, Y. Cheng, L. Ma, Y. Zhang, Stabilizing performance of montmorillonite on fish gelatin-monascorubins system by labyrinth effect, Prog. Org. Coating 170 (2022) 106979.
[31] Y. Xin, K. Huo, H. Tao, G. Tang, P.K. Chu, Influence of aggressive ions on the degradation behavior of biomedical magnesium alloy in physiological environment, Acta Biomater. 4 (2008) 2008–2015.
[32] F. Cao, G.L. Song, A. Atrens, Corrosion and passivation of magnesium alloys, Corrosion Sci. 11 (2016) 835–845.
[33] J.L. Brash, T.A. Horbett, R.A. Latour, P. Tengvall, The blood compatibility challenge. Part 2: protein adsorption phenomena governing blood reactivity, Acta Biomater. 94 (2019) 11–24.
[34] M. Crago, A. Lee, T.P. Hoang, S. Talebian, S. Naficy, Protein adsorption on blood-contacting surfaces: a thermodynamic perspective to guide the design of antithrombogenic polymer coatings, Acta Biomater. 180 (2024) 46–60.
[35] L. Yao, C. He, S. Chen, W. Zhao, Y. Xie, S. Sun, S. Nie, C. Zhao, Codeposition of polydopamine and zwitterionic polymer on membrane surface with enhanced stability and antibiofouling property, Langmuir 35 (2018) 1430–1439.
[36] W. Yang, S. Chen, G. Cheng, H. Vaisocherová, H. Xue, W. Li, J. Zhang, S. Jiang, Film thickness dependence of protein adsorption from blood serum and plasma onto poly (sulfobetaine)-grafted surfaces, Langmuir 24 (2008) 9211–9214.

[37] Y. Zhu, W. Liu, T. Ngai, Polymer coatings on magnesium-based implants for orthopedic applications, J. Polym. Sci. 60 (2022) 32–51.
[38] T. Yang, Z. Du, H. Qiu, P. Gao, X. Zhao, H. Wang, Q. Tu, K. Xiong, N. Huang, Z. Yang, From surface to bulk modification: plasma polymerization of amine-bearing coating by synergic strategy of biomolecule grafting and nitric oxide loading, Bioact. Mater. 5 (2020) 17–25.
[39] Z. Yang, S. Zhong, Y. Yang, M.F. Maitz, X. Li, Q. Tu, P. Qi, H. Zhang, H. Qiu, J. Wang, N. Huang, Polydopamine-mediated long-term elution of the direct thrombin inhibitor bivalirudin from TiO_2 nanotubes for improved vascular biocompatibility, J. Mater. Chem. B 2 (2014) 6767–6778.
[40] Y. Weng, Q. Song, Y. Zhou, L. Zhang, J. Wang, J. Chen, Y. Leng, S. Li, N. Huang, Immobilization of selenocystamine on TiO_2 surfaces for in situ catalytic generation of nitric oxide and potential application in intravascular stents, Biomaterials 32 (2011) 1253–1263.
[41] S.X. Anand, M.C. Kim, M. Kamran, S.K. Sharma, A.S. Kini, J. Fareed, D. A. Hoppensteadt, F. Carbon, E. Cavusoglu, D. Varon, J.F. Viles-Gonzalez, J. J. Badimon, J.D. Marmur, Comparison of platelet function and morphology in patients undergoing percutaneous coronary intervention receiving bivalirudin versus unfractionated heparin versus clopidogrel pretreatment and bivalirudin, Am. J. Cardiol. 100 (2007) 417–424.
[42] G.W. Stone, B.T. McLaurin, D.A. Cox, M.E. Bertrand, A.M. Lincoff, J.W. Moses, H. D. White, S.J. Pocock, J.H. Ware, F. Feit, A. Colombo, P.E. Aylward, A.R. Cequier, H. Darius, W. Desmet, R. Ebrahimi, M. Hamon, L.H. Rasmussen, H.J. Rupprecht, J. Hoekstra, R. Mehran, E.M. Ohman, Bivalirudin for patients with acute coronary syndromes, N. Engl. J. Med. 355 (2006) 2203–2216.
[43] T. Yang, Z. Du, H. Qiu, P. Gao, X. Zhao, H. Wang, Q. Tu, K. Xiong, N. Huang, Z. Tang, From surface to bulk modification: plasma polymerization of amine-bearing coating by synergic strategy of biomolecule grafting and nitric oxide loading, Bioact. Mater. 5 (2020) 17–25.
[44] W. Cha, M.E. Meyerhoff, Catalytic generation of nitric oxide from S-nitrosothiols using immobilized organoselenium species, Biomaterials 28 (2007) 19–27.
[45] L. Jia, C. Bonaventura, J. Bonaventura, J.S. Stamler, S-nitrosohaemoglobin: a dynamic activity of blood involved in vascular control, Nature 380 (1996) 221–226.
[46] Y. Lin, J.E. Spallholz, Generation of reactive oxygen species from the reaction of selenium compounds with thiols and mammary tumor cells, Biochem. Pharmacol. 45 (1993) 429–437.
[47] E.R. Derbyshire, M.A. Marletta, Structure and regulation of soluble guanylate cyclase, Annu. Rev. Biochem. 81 (2012) 533–559.
[48] J. Lei, Y. Vodovotz, E. Tzeng, T.R. Billiar, Nitric oxide, a protective molecule in the cardiovascular system, Nitric Oxide 35 (2013) 175–185.